LHCb 2000-057
Outer Tracker
July 4, 2000

LHCb Outer Tracker prototypes

October 1998 and June 1999 testbeam data analysis

Rutger van der Eijk
NIKHEF, Amsterdam, The Netherlands

Contents

This note describes measurements performed on various prototype modules of LHCb Outer Tracker drift chambers in the test beam periods of 1998 and 1999. Presented are measurements of various drift cell characteristics. The single cell efficiency is shown to be better than 98%. The gas mixture Ar:CF_4:CO_2 (68:27:05) in a 5 mm straw tube is just fast enough to keep the maximum drift time within two LHC bunch crossings. It is shown that 8 mm cells do not satisfy this criterium. The noise in the tested 5 mm prototypes is below 0.2%, the main source of this noise is the amplifier/shaper. Next to presenting the measurements, the test beam setup is described. Furthermore a description is given of the used analysis methods. The same methods will be used to analyse the data taken in 2000. This data will be reported in a seperate note.

1 Introduction

This note describes measurements performed on various prototype modules of LHCb Outer Tracker drift chambers. The data presented here are the combined data of two test beam periods at the CERN PS accelerator. The first test beam period was from October 21 until November 11 in 1998. The second period was from May 31 until June 14 in 1999. Furthermore this note gives a description of the used analysis methods. The same methods will be used to analyse the data taken in 2000. This analysis will be reported in a seperate note.

The main goal was to measure the cell characteristics of the prototype drift chambers to test if they satisfy the design criteria. The double-layer efficiency, i.e. the total efficiency of two staggered mono-layers, has to be nearly 100%. The single cell efficiency therefore also has to be close to 100%. Pattern recognition in the LHCb track reconstruction requires a maximum of two overlapping bunch crossings. Taking into account the propagation time along the wire, this results in a maximum drift time in a cell of 40ns to 45ns depending on the size of the drift chambers. The requirements on resolution are less stringent but should not exceed 200 μm. Furthermore, noise and crosstalk should be kept as low as possible. The various characteristics depend of course on the applied high voltage, threshold and gas mixture. Therefore the measurements of the above quantities have been performed as function of these parameters.

1.1 Iterative procedure

In the data analysis we are faced with the circular dependency of various quantities and methods. In order to reconstruct and fit tracks we need a proper t0-calibration to remove individual channel offsets, a distance-drift-time-relation (RT-relation for short) to convert the measured drift time in a distance to the wire, a calibrated geometry to know the position of the drift cells and a cell resolution in order to calculate a proper χ^2. However to calibrate the geometry, to auto calibrate the RT-relation (see [1]) and to determine the resolution, we need reconstructed tracks. To solve these chicken and egg problems we follow a stepwise iterative procedure. For all observables we assume initial values, reconstruct tracks assuming these values to be correct, and next use these tracks to update the observables. We repeat this procedure until the required accuracy is obtained. The numbers presented and figures shown in this note are obtained after the "final" iteration step.

2 Experimental setup

As mentioned before this document describes the measurements performed on various LHCb Outer Tracker prototype drift chambers at two test beam periods at the CERN PS accelerator. This chapter summarises the experimental setup, i.e. the particle beam, the magnet, the tested prototype chambers, the electronics and the software.

2.1 Particle beam

Both tests were performed at the PS accelerator at CERN. The PS accelerates and stores protons up to an energy of 25 GeV. Part of these protons are extracted from the PS into the "East Area" where via two targets five secondary beams are produced. Both tests were performed at the secondary beam called T7. The PS operates with a "super-cycle" of 14.4 seconds delivering 1 to 3 spills of particles on the secondary beam production targets with a duration of 300 to 500 msec. The maximum number of protons on a single target is $2 \cdot 10^{11}$ protons per spill.

Via beam magnets and slits the content, intensity and shape of the T7 beam could be controlled. During most of the tests we used a 9.5 GeV π^- beam covering almost the full acceptance of the detectors. Because the data acquisition electronics appeared to have major problems[1] with even a fraction of the design trigger rate of 100kHz, we tried to keep the particle rate as low as possible. The minimum achievable beam intensity was about 6000 particles per spill ($\simeq$20kHz instantaneous rate for 300 msec).

2.2 Magnet

In order to test the drift behaviour in a magnetic field the warm magnet MN22 was used. This magnet can supply a maximum field of 1.37 Tesla within the gap volume of $1.0 * 1.0 * 0.5m^3$ between the coils. Outside the magnet a stray field is observed.

2.3 Drift chamber prototypes

During the two test beam periods different prototype drift chambers have been tested. The prototypes differ in shape, material and construction method. For a detailed description on the operation of drift chambers see e.g.

[1] Especially the 1998 test beam period suffered from data acquisition problems. See section 3.1 for a more complete description.

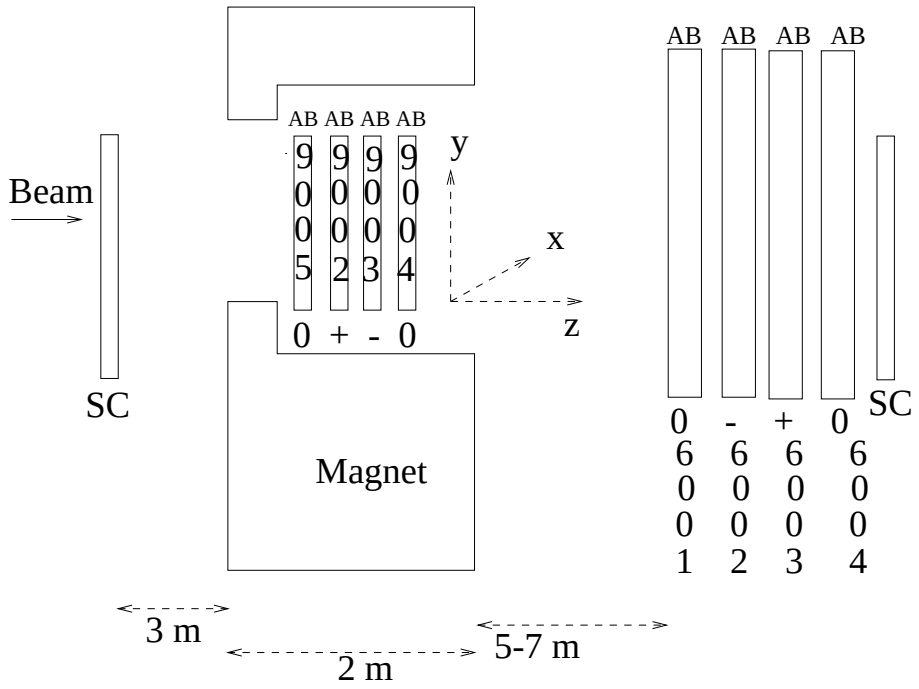

Figure 1: Experimental setup of chambers, magnet and scintillators(**SC**) in the 1998 test beam period. The "planks", i.e. two staggered single layers labeled A and B, are oriented vertical(**0**) or under a stereo angle of +or -5 degrees.

[1, 2]. The tested prototypes and their positioning in the beam are described below.

2.3.1 October 21 - November 11 1998 test beam period

The 1998 setup consists of two stations. Both stations are made out of four "planks", where every "plank" consists of two staggered mono-layers. The total setup is shown in figure 1. All drift cells have a thickness of 5 mm. Station 1 is placed in the magnet. It contains the planks labeled 9002 to 9005. These planks contain honeycomb shaped drift cells with a 9 mm pitch and 8 mm width (see figure 2). They have a length of ∼30 cm. Station 2 is placed further downstream and consists of the planks labeled 6001 to 6004. These planks have honeycomb shaped drift cells with a diameter of 5 mm, a pitch of 6 mm and a length of ∼1 m. The four planks within a station were oriented such as will likely be the case within a standard LHCb station, i.e. a vertical plank, a +5 stereo angle plank, a -5 stereo angle plank and another

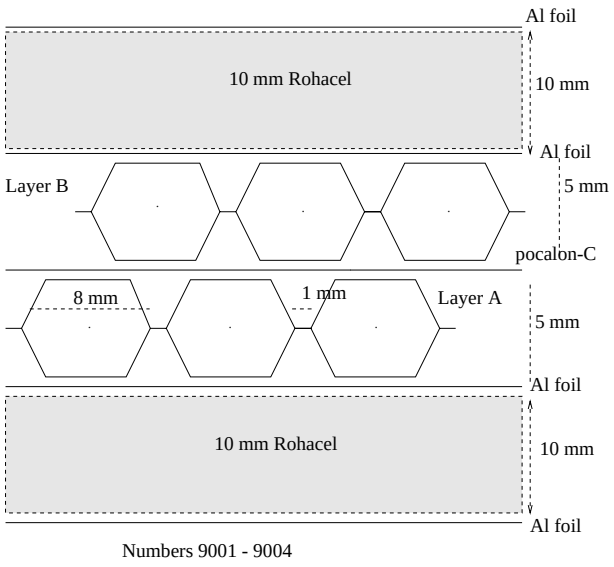

Figure 2: Cross section of 8 mm honeycomb planks 9001 to 9004. Every plank consist of two mono-layers labeled A and B.

vertical plank. For a more detailed description of the setup see [3].

2.3.2 May 31 - June 14 1999 test beam period

The 1999 setup consisted of three stations (see figure 3 for an overview of the total setup.) The first station is built out of 5 straw tube planks and is positioned in the magnet. The cells have a diameter of 5 mm, a pitch of 6 mm and a length of approximately 30 cm. They are labeled 6030 to 6034. Connected to station 1 is one mono-layer of a new drift chamber type, the so called "Carbon-Coated Drift chamber" (see [4] for a description of these "FMUL"-chambers). The second station consists of the same planks 9002 to 9005 used in the 1998 test beam period. The difference with the 1998 setup is that planks 9002 to 9004 are now placed vertical. Plank 9005 is placed horizontal and only mono-layer A is read out. Another horizontal plank of 9 mm pitch (9001) is placed horizontal as the first layer of station 3. The rest of station 3 is built out of 4 long ($\sim$1 m) honeycomb planks with 5 mm diameter and 6 mm pitch. They are labeled 6005 to 6008. For a more detailed description of the setup see [5].

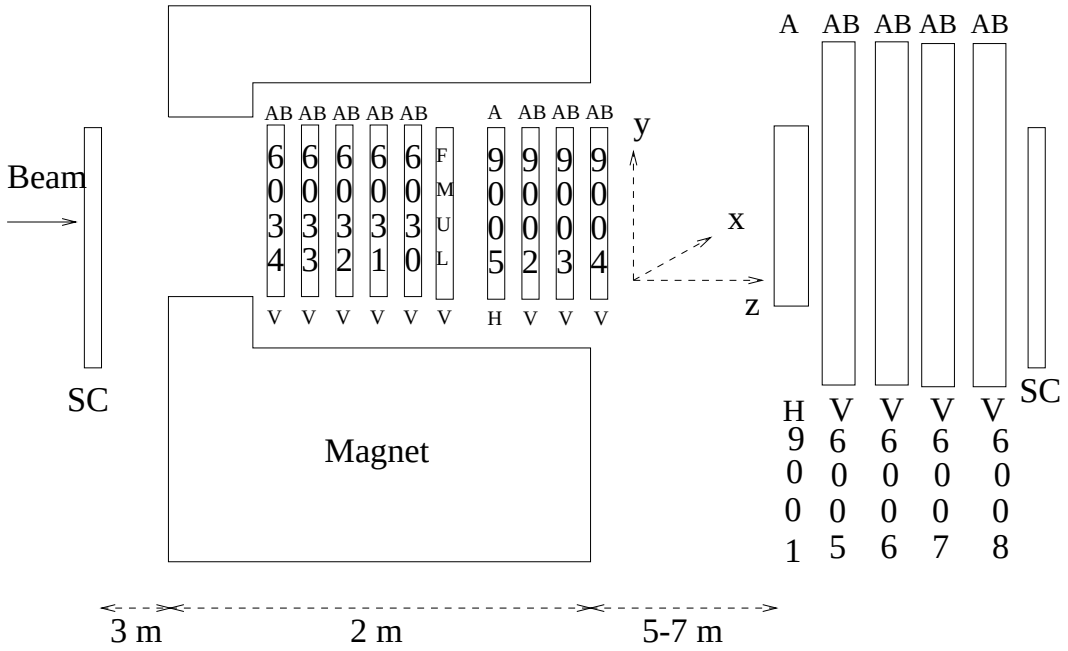

Figure 3: Experimental setup of chambers, magnet and scintillators in the 1999 test beam period. The "planks" are oriented vertical(**V**) or horizontal(**H**).

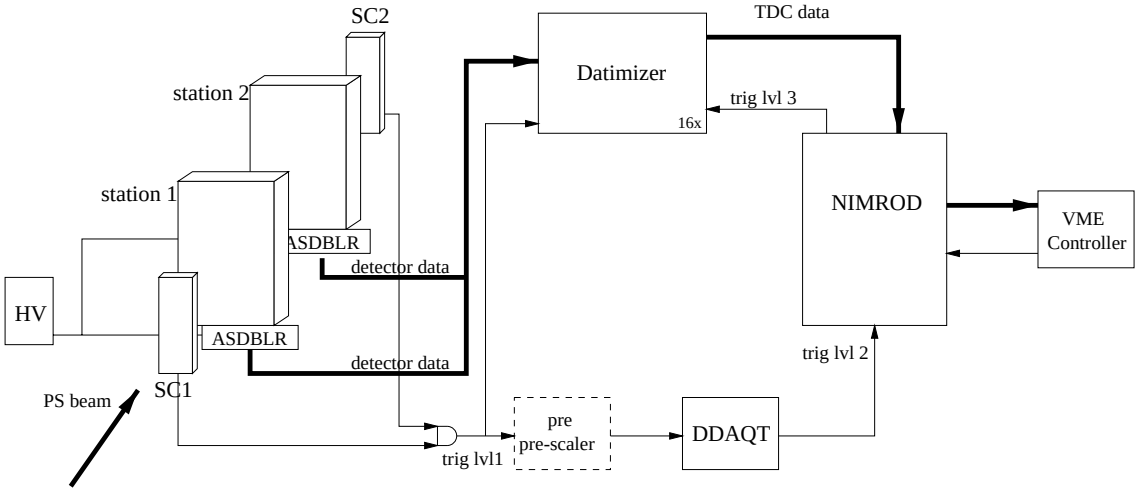

Figure 4: Block scheme of electronics used in the test beams.

2.4 Electronics

The data acquisition electronics used in the test beams consists of several components. A block scheme of the electronics setup is shown in figure 4, the individual components are briefly described below. For a more detailed description of the electronics see [6].

- Directly connected to the detector modules is a board which supplies the high voltage and performs the first step in the signal readout. On the board so called ASDBLR chips are mounted. The input to the "**A**mplifier **S**haper **D**iscriminator with **B**ase**L**ine **R**estoration" chips is the direct signal from the cell wires. The output is a digital signal, i.e. no pulse height and shape information is kept. Every ASDBLR chip handles 8 readout channels. See [7] for a more detailed description of this amplifier. See [8] for a study on the operational properties of the chip for the LHCb Outer Tracker.

- The digital output of the ASDBLRs is further processed by the datimizer boards [9]. The most important component of a datimizers board is the TDC chip. We use the 32 channel TDC32 chip developed at CERN [10]. This chip provides a time to digital conversion with a binning of 0.78 ns, a data buffering of 256 words deep and trigger matching logic. It is highly configurable for the needs of specific experiments via a JTAG[11] interface. We used the TDC in a "data driven" mode and triggered on the leading edge of the signal from the ASDBLRs.

- The data of the TDCs of the several datimizer boards are combined to a single event by a NIMROD [12] module. The NIMROD has originally been designed for the ATLAS muon chambers to collect the data of a maximum of 16 Front End Links (in our case the datimizers) and send this this data via a high speed link to a higher level data acquisition module. Furthermore it receives the clock trigger and timing information from the DDAQT module (see below) and distributes this to the TDCs. The NIMROD is a VME module.

- The VME controller is a Motorola processor running a real time Lynx OS system. On the processor a data acquisition system is running (see section 2.5 for a brief description of this Low Level DAQ software) which steers the various VME components. The main task is the communication with the NIMROD. Via the VME bus the data is read out[2] and stored locally on disk.

[2]As mentioned the NIMROD is designed to output its data via a fast optical link to

- The coincidence of the signal of 2 scintillators, one placed before and one after the stations, is used as a primary trigger. This primary trigger signal is fed into the trigger processor unit called DDAQT (see [13]). In addition the primary trigger is fed into a dedicated TDC channel on a datimizer board to provide a fine time measurement (i.e. 25/32 ns) of the trigger signal. The DDAQT has the possibility to reduce the trigger rate by outputting every n^{th} trigger of the input trigger rate. This secondary trigger signal serves as input for the NIMROD. Because the DDAQT did not work properly in the 1998 test beam we used a "hand-made" NIM-circuit (*pre-pre scaler*) to reduce the trigger rate.

2.5 Software

The software used in the tests consists of two parts. One part performs the direct steering of hardware modules and the retrieval of event data from the NIMROD. This **L**ow **L**evel **DAQ**(LLDAQ) software was based on existing software for the steering of similar electronics modules for the L3+Cosmics experiment. See [14] for a description of this LLDAQ software. On top of the LLDAQ software an online monitoring and data analysis framework was written. This software is written in C++ within a ROOT[15] framework. The test beams can be online controlled from Graphical User Interfaces, i.e. start/stop of a run with the appropriate settings, a monitor of run and DAQ statistics, an event display and a histogram display. All data analysis is done in a analysis computing philosophy similar to the general LHCb software, i.e. Gaudi [16] implemented within ROOT. For a more detailed description of the analysis and monitoring software see [17].

higher level data acquisition units. Because these units were not avalaible we read the data via the VME bus, which is a feature available for testing the NIMROD. This back-door readout of the data proved to be the bottleneck in the data transfer rate of the data acquisition system.

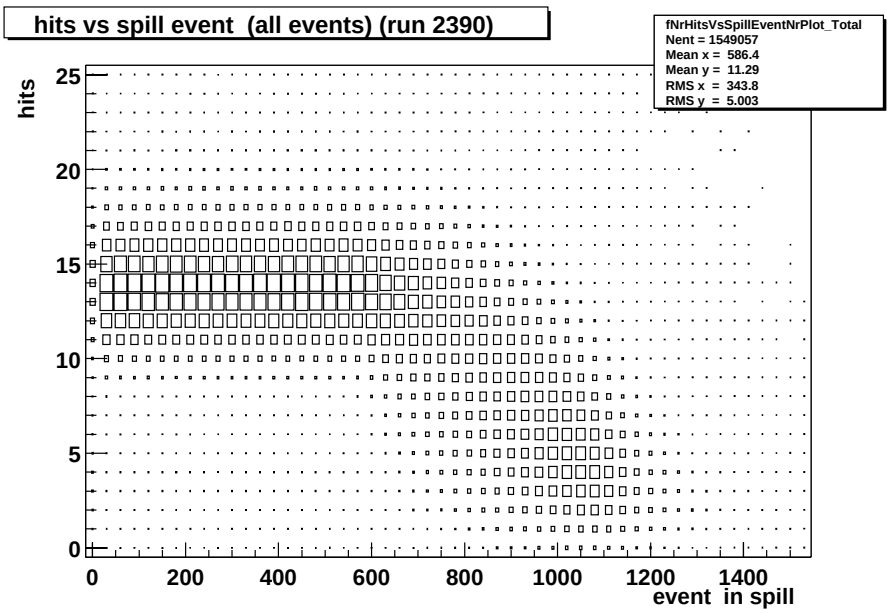

Figure 5: The number of hits in an event vs. the event number in the spill for the standard run. On average we had 6000 triggers per spill in this run. Visible is the drop in number of hits at about "spill event" 600.

3 Data

3.1 DAQ problems

Both test beam periods suffered from major problems with the data acquisition electronics. The main problem was the loss of parts of the event data somewhere in the data acquisition chain. Detailed study showed that there were several sources of this data loss, mainly in (the combination of) the datimizer and NIMROD.

One clear proof of the data loss in the data acquisition can be seen from figure 5. In this figure the number of hits in an event vs. the event number in a spill is plotted. Clearly visible is the drop in number of hits at about spill event 600. The event number at which the drop occured depended on the settings of the DDAQT module, the NIMROD and the datimizer module.

A complication in the data analysis is that not all data acquisition problems were flagged inside the data. As a consequence various stringent quality selection criteria had to be applied resulting in a limited amount of data avail-

able[3]. Therefore not all detector prototypes presented in section 2.3 could be properly tested. An example of one of the applied data quality cuts is the selection of only the first n events within a spill[4]. These cuts might still bias the results presented in the following chapters. This should be regarded as a systematic error (e.g. the detector efficiency might be underestimated due to a data acquisition inefficiency).

3.2 Data samples

The gas dependency results presented in section 4 were obtained with the 8 mm honeycomb modules 9002 to 9005. In the same section some results of the "carbon-coated drift chambers"[4] are shown. All other results were obtained with the 5 mm straw tube modules 6030 to 6034.

All results with no specific dependency on high voltage, threshold, gas mixture and magnetic field, i.e. efficiency, noise, TR-relation, resolution are obtained using one specific data sample. This data sample of the 1999 testbeam (run 2390) was taken under the following conditions:

- 10 layers of 5 mm straw tubes (modules 6030 to 6034).
- particle flux: $\sim$20kHz for 0.3sec.
- gas mixture: Ar:CF_4:CO_2(68:27:05).
- no magnetic field.
- HV = 1650V.
- V_{tresh} = 2.4V (corresponds to 6 fC).

This run is from now on referred to as the *standard run*.

[3]In most of the 1998 runs only 5% of the data could be used.
[4]n=500 in case of the run in figure 5

4 Drift times

4.1 Drift time spectra

The starting point of the characterisation of prototypes is the drift time spectrum of the drift chamber. In figure 6 drift time spectra for 8 mm honeycomb cells of the modules 9002 to 9005 are shown for various settings. Due to the mentioned data acquisition problems the statistics is limited. From this data set noise hits could not be removed by using reconstructed tracks because tracks could not be properly reconstructed. The top plot shows the spectrum for the (by now) standard gas mixture Ar:CF_4:CO_2(68:27:05) without magnetic field. The maximum drift time is approximately 55 ns. The middle plot shows a spectrum for the same cells with the magnetic field turned on to 1.0 Tesla. As expected the result is a different shape of the spectrum and a larger maximum drift time. The bottom plot shows the drift time spectrum for a gas mixture without CF_4 (i.e. 80% Argon and 20% CO_2). Clearly this gas mixture is slower than the standard mix (note the different time-axis scale.)

In figure 7 the drift time spectrum of the carbon-coated drift chambers is shown for the standard gas mix and no magnetic field. Within statistics the shape is the same as the spectrum for the 5 mm straws of the standard run as shown in figure 8. Note that, contrary to the other spectra, in figure 8 noise has been rejected by requiring the hits to be on the reconstructed track.

4.2 Maximum drift time

Because of the LHC bunch crossing interval of 25 ns we need a fast drift gas. Pattern recognition in the LHCb track reconstruction requires a maximum of two overlapping bunch crossings. Taking into account the propagation time along the wire this results in a maximum allowed drift time of 40 ns to 45 ns, depending on the lenght of the drift chambers. From a drift time spectrum the maximum drift time can be extracted. Several extraction methods have been tested. In the figures shown selected start en stop time of the spectra are indicated.

In Table 1 the maximum drift time for various gas mixtures with and without magnetic field in the honeycomb chambers is shown. The third column shows the measured maxima from the test beam. The fourth column contains maximum drift times from a monte carlo study using the simulation program Garfield [18]. Within the limited statistics available, measurement and simulation agree. Only the gas mixture without CO_2 (i.e. 71% Argon and

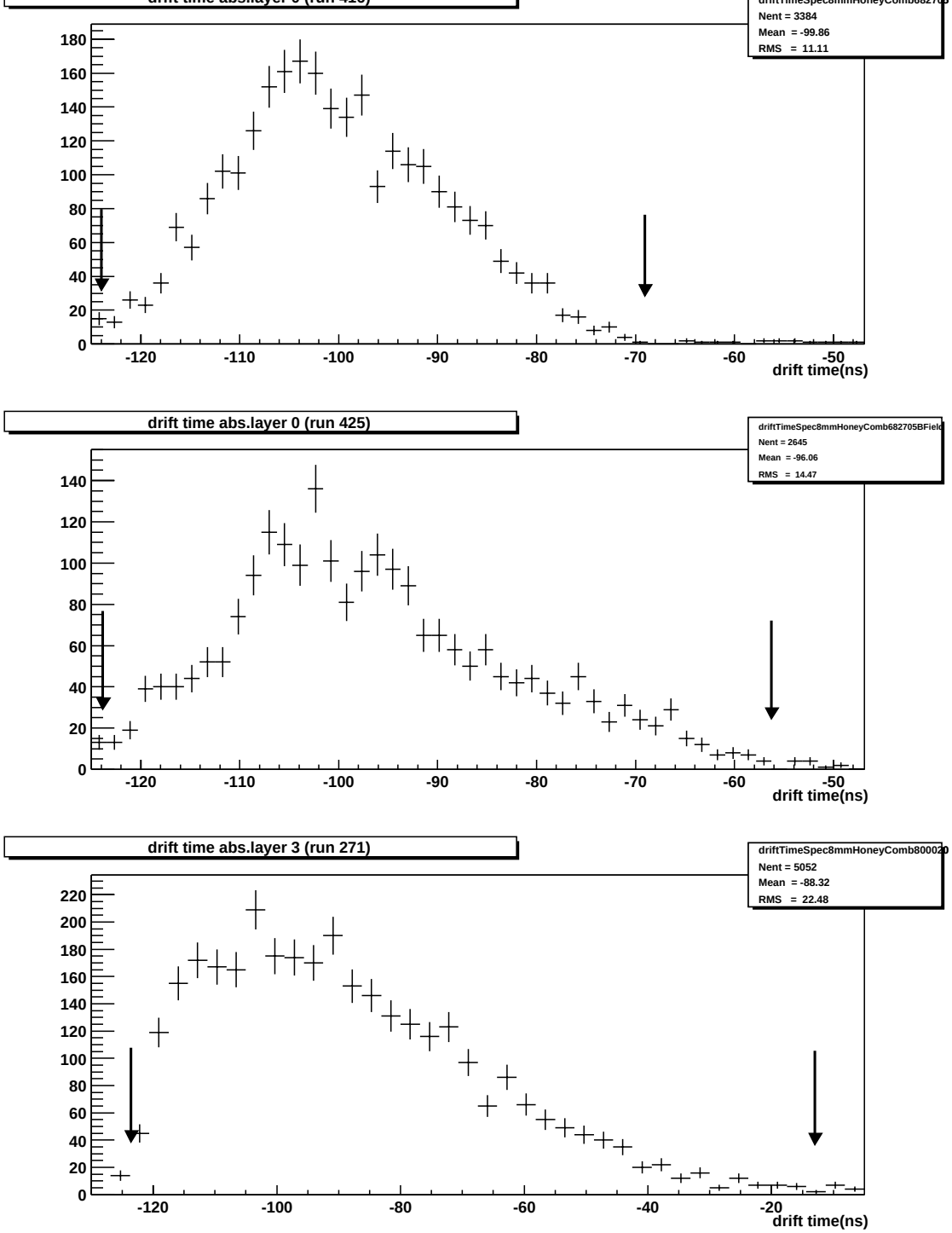

Figure 6: Drift time spectra for 8 mm honeycomb drift cells from the module series 9002 to 9005. **A)** Mono-layer 9005A with gas mixture Ar:CF_4:CO_2(68:27:05), B = 0.0 Tesla and a treshold of 9 fC. **B)** Mono-layer 9005A with gas mixture Ar:CF_4:CO_2(68:27:05), B = 1.0 Tesla and a treshold of 9 fC. **C)** Mono-layer 9002B with gas mixture Ar:CF_4:CO_2(80:0:20), B = 1.0 Tesla and a treshold of 9 fC.

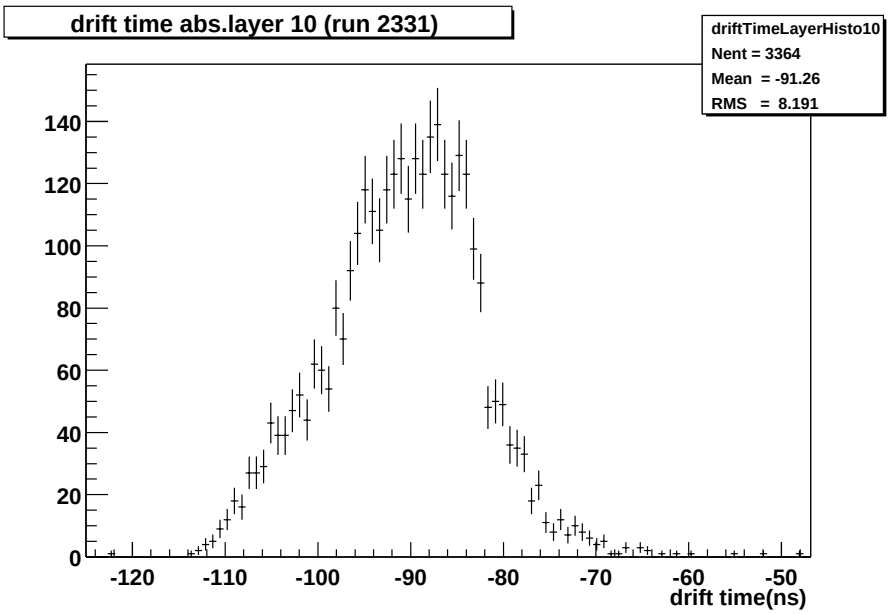

Figure 7: Drift time spectrum for carbon-coated drift chambers with gas mixture Ar : CF_4 : CO_2(68:27:05), no magnetic field and a treshold of 7 fC.

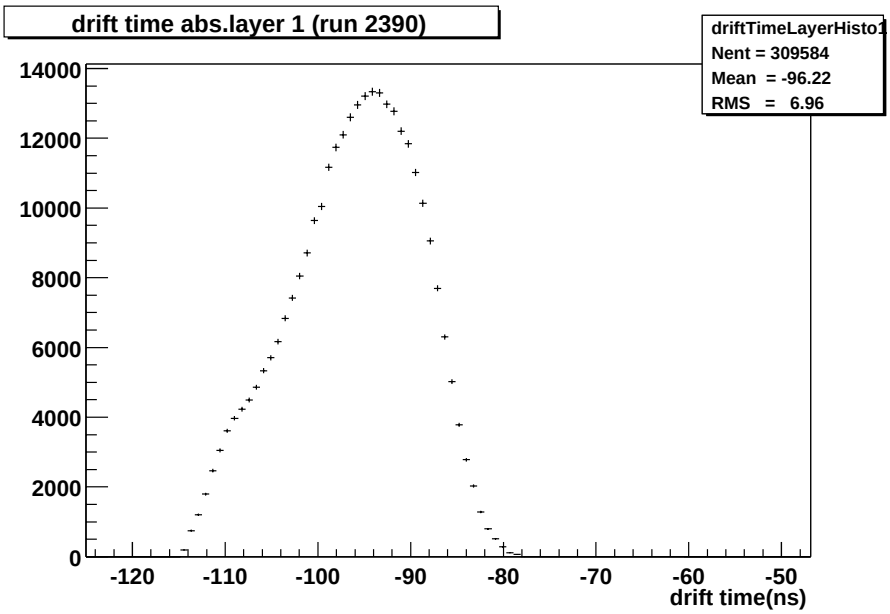

Figure 8: Drift time spectrum for 5 mm straw tubes in the standard run.

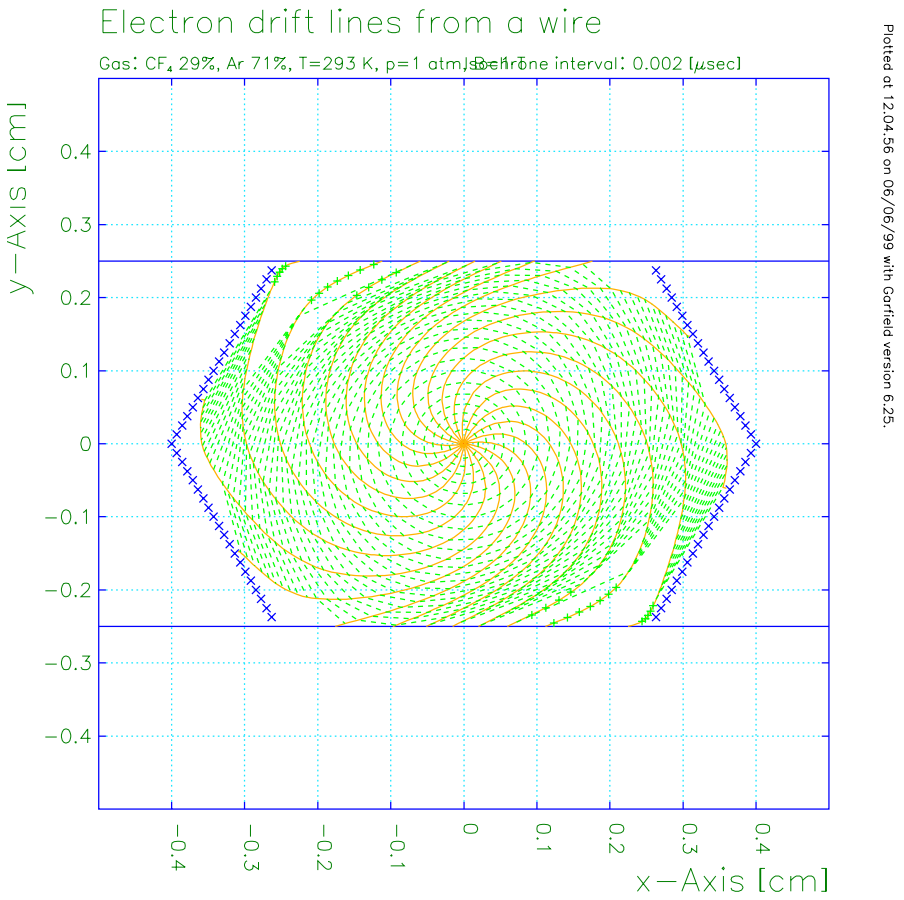

Figure 9: Simulated drift lines in a 8 mm honeycomb cell with the fast gas mixture 71% Argon and 29% CF_4 in a 1.0 Tesla magnetic field. Shown are drift lines and equipotentials.

Gas mixture ($Ar:CF_4:CO_2$)	B_y (Tesla)	T_{max} (ns)	
		Test beam	Garfield
71:29:0	0.0	~ 45	40±4
	1.0	> 100	120±20
68:27:5	0.0	~ 55	60±5
	1.0	~ 65	60±5
81:14:5	0.0	~ 60	64±4
	1.0	~ 90	80±8
88:7:5	0.0	~ 70	70±5
	1.0	~ 90	88±10
80:0:20	0.0	~ 110	110±30
	1.0	~ 110	125±40

Table 1: Simulated and measured T_{max} (in ns) for a 8 mm honeycomb chamber (planks 9002 to 9005) for various gas mixtures for magnetic field along the wire direction (vertical).

29% CF_4) just stays within the required maximum of 45ns drift time in case no magnetic field is applied. However, if the field is turned on the increase in drift time is large, and even larger than for relatively slow drift gases. This is caused by the increased Lorentz angle resulting in a longer effective drift distance (see figure 9 for simulated drift lines in this gas mixture with a 1.0 Tesla magnetic field.).

Because the maximum drift time in 8 mm honeycomb modules is to large, prototypes with a smaller cell size were developed. In Table 2 the simulated maximum drift time in a 5 mm straw tube in the standard gas mixture is shown for various magnetic field values and directions. Table 3 shows the measured maximum drift times for the 6001 to 6004 straw tubes in the 1999 test beam. Unfortunately the magnet used in the test beam could not exceed 1.4 Tesla. The measured and simulated values are within good agreement. From the simulated drift times we can therefore conclude that 5 mm straw tubes in the standard gas mixture can stand a maximum of 1.6 Tesla to stay within 45 ns of maximum drift time.

4.3 t0 calibration

In order to use a drift time as a measure for the shortest distance to the wire of a passing particle (see section 7) we need to calibrate the time offset present in the recorded time. One can distinguish a global time offset and a local time offset. The global time offset is an offset which can be freely

		B_z **(Tesla)**				
		0.0	**0.5**	**1.0**	**1.2**	**1.4**
B_y (Tesla)	**0.0**	27				
	0.5	26				
	0.8	30	32			
	1.0	32	34	38		
	1.2	35	36	40	42	
	1.4	39	39	43	44	47
	1.6	43	43	46	47	49
	1.8	48	47	49	50	52
	2.0	54	52	52	53	55
	2.2	62	57	56	57	59

Table 2: Simulated T_{max} (in ns) for a 5 mm straw tube in a Ar:CF_4:CO_2-(68:27:05) gas mixture for a magnetic field with Y (along the wire) and Z (perpendicular to the wire) components.

B_y **(Tesla)**	T_{max} **(ns)**
0.0	28 $\pm$1
1.0	32 $\pm$1
1.4	37 $\pm$2

Table 3: T_{max} as function of the magnetic field as measured in the 1999 test beam for the 5 mm straw modules with an Ar:CF_4:CO_2(68:27:05) gas mixture.

chosen as long as the RT-relation uses the same offset. The local offset is the time offset of individual channels with respect to the global offset used for the RT-relation. Several methods have been tested to calibrate the local time offset. In the end the average time of the drift spectrum proved to be sufficient.

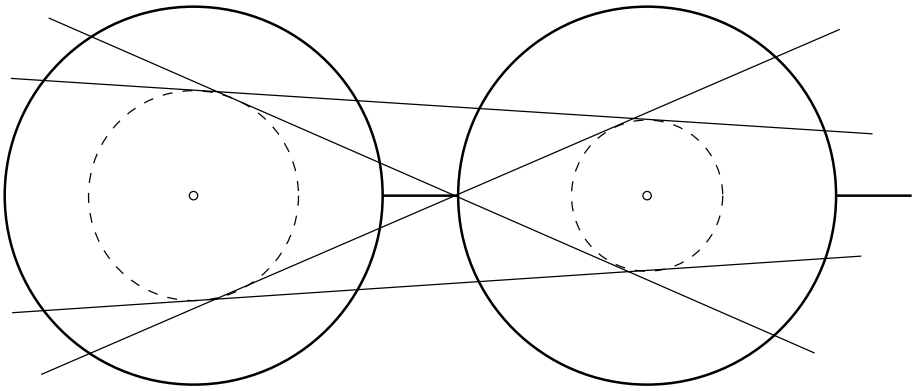

Figure 10: Four possible hit pairs due to left/right ambiguity.

5 Track reconstruction

In order to establish the primary goal of the experiments, i.e. test and measure cell characteristics of prototype drift chambers, we need to know if a particle traversed a certain cell. This section deals with the reconstruction of the particle trajectories. Track reconstruction can be split in track finding and track fitting. Track finding deals with finding the hits belonging to a single particle, i.e. the pattern recognition. Track fitting results in the best estimate of the particle trajectory from the measurements.

As mentioned in section 1 we follow an iterative and step wise procedure in the determination of the cell characteristics. In the track reconstruction step the time offset, the alignment, the RT-relation and the resolution dependence on the drift time are assumed to be given, i.e. fixed. In a next calibration step the found tracks can be used to improve upon e.g. the RT-relation.

5.1 Track finding

To reconstruct the tracks we need a track finding algorithm that combines hits created by a single passing particle and discards noise hits or hits from other particles. A track finding algorithm should also take care of solving the left/right ambiguities. The basis of the algorithm we used is an idea of H.Tolsma [1] which is also described in [19]. We used a slightly modified version with the following steps:

- Combine every hit with every other hit. Make 4 hit pairs, one for each left right ambiguity (see figure 10).

- Use the pair with the longest distance between the wires as the first initial track candidate. All remaining hits are tested for the residual w.r.t. the track candidate. If the residual is smaller than a certain value the hit is added to the track. In case both ambiguities satisfy the addition criteria the ambiguity with the smallest residual is chosen.

- The created track is tested for validity, meaning a minimum number of hits on the track. If the track candidate is not valid it is discarded. If it is valid the candidate is kept in a track candidate list.

- The hit pairs used by the found track are discarded. The above procedure is repeated on the remaining hit pairs until no pairs are left.

- The list of found track candidates is further reduced by requiring hits to be only used by one candidate. This is achieved by fitting the candidates and selecting the track with the highest quality (see section for a definition of track quality 5.2). All hits used by this track are removed from the other candidates.

- The remaining candidates are checked on their validity. If after that any valid candidates remain the reduction procedure is repeated, starting again with the highest quality candidate.

The main difference w.r.t the algorithm used in [19] is the hit addition on a residual basis without re-fitting the track. In this way the hit addition is not biased by the order of the hits, hence no randomisation is necessary.

5.2 Track fitting

The track fit aims to produce the best estimate of the particle trajectory from the measurements. The trajectory is parametrised by a set of *track parameters*. The parameters have to be chosen such that, in the various mathematical operations involved, the correlations between them are minimal.

We used the Kalman Filter Technique [20] to fit the track parameters. The Kalman Filter has several advantages over a global fit. For a full description of the Kalman Filter applied to track reconstruction in high-energy physics see e.g. [21] and [22]. Below we show how we have applied the technique to our setup[5].

[5]The main advantages of the Kalman Filter Technique over a "global fit" are the efficient way of dealing with multiple scattering and energy loss, the ability to combine track fitting and finding as measurements can be added progressively. In addition it is

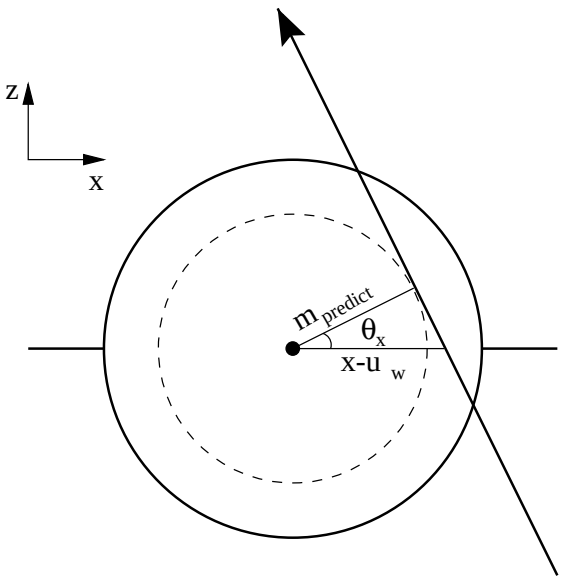

Figure 11: Projection of track parameters into the measurement space of a straw tube cell.

In the analysis of the 5 straw tube modules of the standard run (see section 3.2) we assumed all wires to be parallel (which is the case if we ignore possible miss alignments in the angles), in which case the setup can be seen as 2-dimensional. In this case we have chosen the set of track parameters

$$\mathbf{x} = (x, t_x)_z$$

where x is the x-position and t_x the slope ($=dx/dz$) of the track at a certain z position. In case there is no magnetic field and if we ignore multiple scattering and energy loss[6] we can assume a linear *track model*. The *propagation* of the track parameters from one z position to another can simply be achieved by

$$\mathbf{x_{z'}} = F\mathbf{x_z} = \begin{pmatrix} 1 & z'-z \\ 0 & 1 \end{pmatrix} \begin{pmatrix} x \\ t_x \end{pmatrix}_z$$

where F is the so called propagation or transport matrix. The covariance matrix C of the track parameters is then propagated by

a very fast algorithm since the mathematics does not require the inversion of matrices with the dimension of the number of track parameters. Within the general LHCb track reconstruction program the Kalman Filter technique is used. Hence within this analysis we have used the technique.

[6]The radiation thickness is approximately 0.6% X_0 per plank.

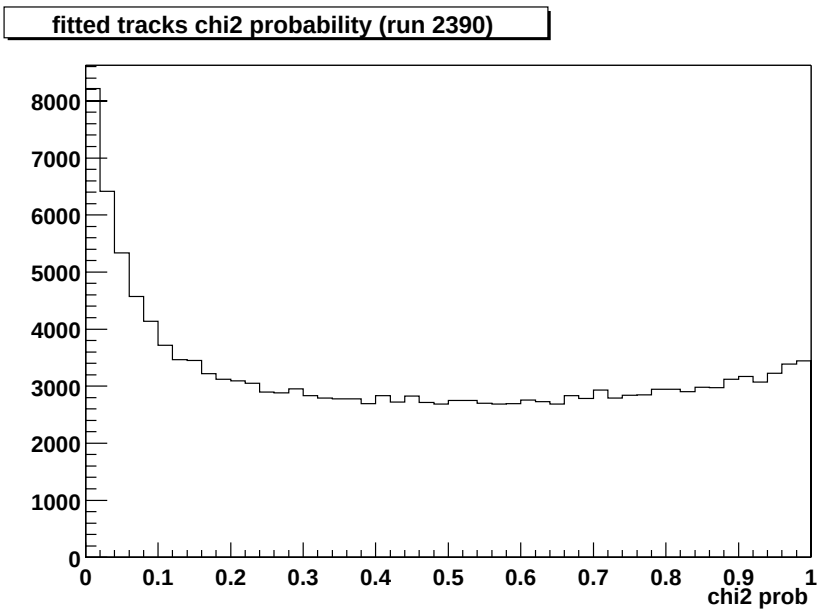

Figure 12: Track fit χ^2 probability for standard run.

$$C_{z'} = FCF^T$$

Within the track fit we use the shortest distance to the wire as the quantity measured by a drift cell. In order to predict this distance from the track parameters we use the *projection* relation

$$m_{\text{predict}} = h(\mathbf{x}) = (x - u_w) \cdot cos\theta_x$$

where u_w is the the x-position of the wire and θ_x the slope of the track (see figure 11) at the z-position of the drift cell.

In the end the Kalman filter applied to tracking is equivalent to a least squares fit. In figure 12 the χ^2 probability function $P_s(\chi^2)$ for the track fit in the standard run is shown. If the errors are Gaussian this should be a flat distribution. It can be seen that this is not the case as will be further explained in section 8.

In track finding the χ^2 of a track is not a good criterion to chose between track candidates, as it tends to bias towards tracks with a low number of hits. The criterion we therefore use is the track quality Q (see [23]), which is defined as

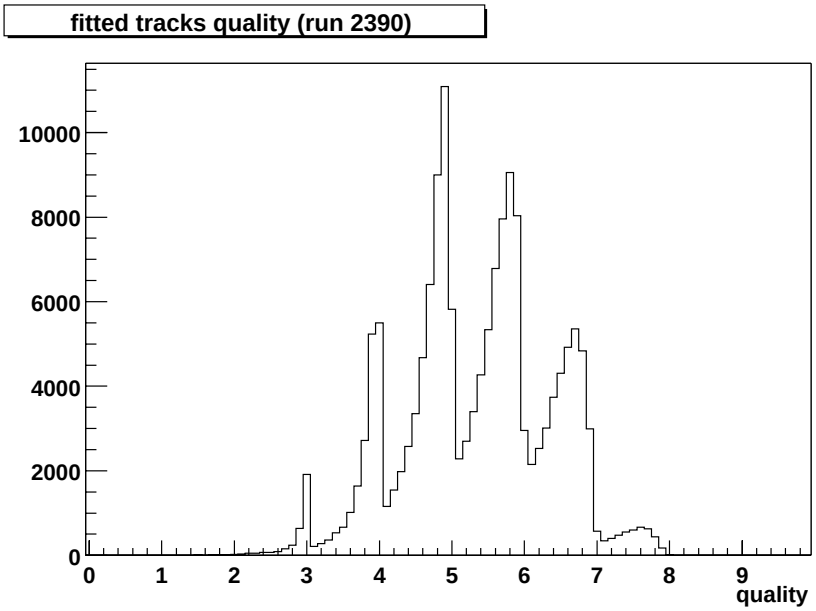

Figure 13: Track fit quality distribution for 8 straw layers in the standard run.

$$Q = n - w \sum_{i=1}^{n} \chi_i^2$$

where n is the number of hits, χ_i^2 the χ^2 contribution of the i^{th} hit to the complete track and w a weight factor. The weight factor is taken to be 0.1 which on average corresponds to adding a hit to a track only if its χ^2 contribution is less than 10. See figure 13 for the track quality of tracks fitted in 8 straw chambers. Clearly visible are the peaks for the various numbers of hits on the tracks.

6 Alignment

Tracks are used to measure the cell characteristics of prototype drift chambers. To be able to reconstruct tracks with enough accuracy the chamber positions should be well known. The positions of the chambers where determined in two steps: manual alignment followed by a software alignment procedure.

A rough alignment of chambers was achieved by manually measuring the positions with a ruler and theodolite. On each plank a marker was attached. Furthermore planks were grouped to form stations. On every station-frame also a marker was attached. Finally somewhere in the lab an origin was chosen and marked as such. After positioning the detector the manual aligment procedure now consists of: measuring the position of all station markers w.r.t. the origin in the lab, followed by measuring the position of all plank markers w.r.t. its station marker. A positioning of wires in a layer w.r.t. wires on another layer in the same station of $\sim$ 2 mm was achieved. The manual station positioning was accurate to about $\sim$0.5 cm.

To improve this alignment beyond the estimated single cell resolution of $\sim$200 μm a simple software alignment procedure was performed. Assuming that the manual alignment gives sufficient accuracy to be able to reconstruct tracks, we can calculate the residual between the measured drift coordinate and the distance of the reconstructed track to the wire[7]. In case the chambers are perfectly aligned we expect the residual distribution to be centered at zero. In case of a misalignment we expect an offset from zero in this distribution. The software alignment procedure aims at minimizing the offsets for all chambers. In this way an alignment better than 50 μm was achieved.

[7]Clearly here we need already an initial RT-relation and t0. Again we follow an iterative procedure, where within one alignment step a fixed RT-relation and t0 is assumed.

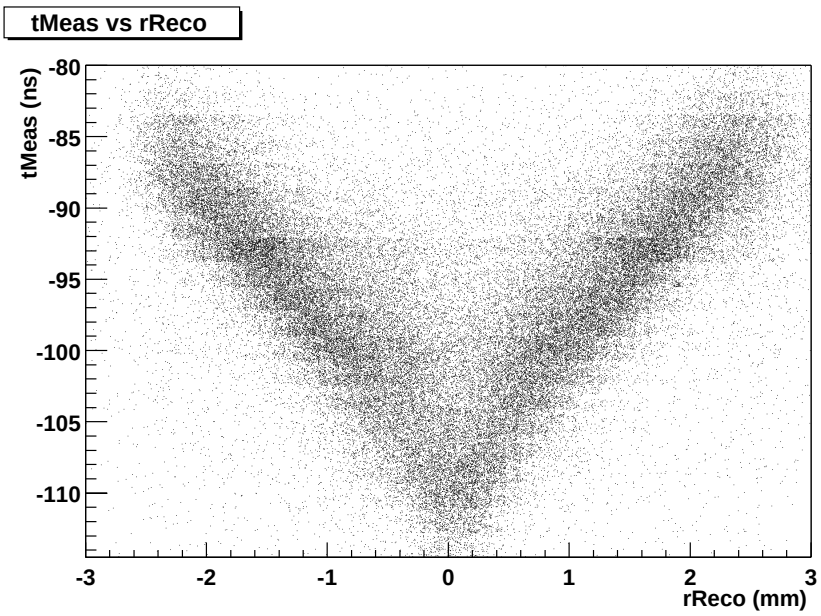

Figure 14: Measured drift time versus predicted distance to wire from reconstructed tracks for the 5 mm straw tubes in the standard run.

7 RT-relation

When an ionising particle traverses a drift cell primary ionisation clusters are created. A drift chamber measures the time of arrival of the closest cluster. For track reconstruction we are, however, interested in the closest **distance** of approach between the traversing particle and the wire, which is not necessarily the same as the position where the closest cluster was produced. We therefore need a relation between the **measured** drift time and the estimated distance of closest approach, i.e. the distance-drift-time relation (RT-relation for short). In figure 14 a scatter plot of measured drift time versus the reconstructed distance to the wire is shown.

Several approaches can be followed to determine the relation between (drift) distance and (drift) time. In fact there is a difference between a distance-time and a time-distance relation. For a track **fit** the distance of closest approach is used as an input, hence one needs a RT-relation. However in if one is interested in the drift cell behaviour a TR-relation is more appropriate because one wants e.g. to know how a cell behaves at a certain distance from the wire. In this note we have chosen to describe the determi-

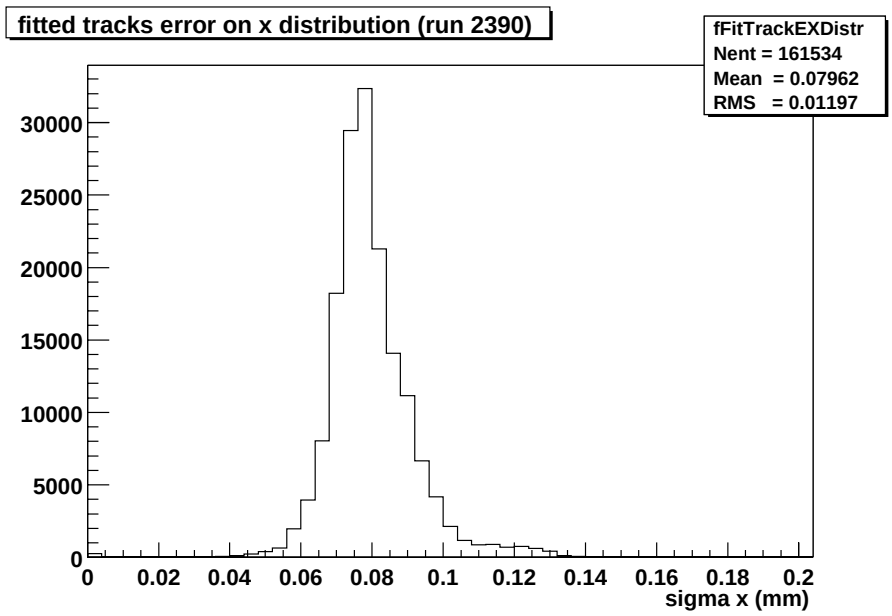

Figure 15: Distribution of the error on r_{reco} in the test layer for the 5 mm straw tubes in the standard run.

nation of the relation directly needed in track fitting, i.e. the RT-relation[8]. The task is to find a relation giving on average the best estimate of the distance of closest approach r_{real} from a measured drift time t_{meas}. In order to achieve this we perform a likelihood fit.

Input to the fit is a set of measurements $(t_{meas}, r_{reco})_i$, where r_{reco} is the signed reconstructed distance of closest approach of a track reconstructed from all layers except the one under study. For every event we calculate the likelihood $P(t_{meas}|r_{reco})$ that it occurs. Since we do not know the true distance of closest approach r_{real} we split the probability in two terms and integrate over all possible values of r_{real}.

$$P(t_{meas}|r_{reco}) = \int_{-R_{max}}^{R_{max}} P(r_{reco}|r_{real})P(t_{meas}|r_{real})dr_{real}$$

The term $P(r_{reco}|r_{real})$ represents the smearing on r_{reco} with respect to the true value due to the finite accuracy of the reconstructed track parameters.

[8]The drift cell behaviour is under study in a separate analysis. This analysis studies, for example, the positioning of the primary ionisation clusters. It also determines the t_{meas}-r_{PI}-relation, i.e. the "true" TR-relation. Here r_{PI} is the distance of the closest primary ionisation cluster to the wire. This analysis will be described in a separate note.

We have assumed a Gaussian distribution of this smearing. In figure 15 the distribution of the error on r_{reco}, resulting from the track fit, is shown.

The second term, $P(t_{meas}|r_{real})$, represents the probability that a measured time t_{meas} occurs if the closest distance of approach was r_{real}. We approximate this probability with a Gaussian around the measured distance r_{meas}.

$$P(t_{meas}|r_{real}) = Ne^{\frac{(r_{meas}-r_{real})^2}{2\sigma_{res}^2}}$$

Here r_{meas} is a function of t_{meas}, i.e. the RT-relation f_{RT} that is fitted.

$$r_{meas} = f_{RT}(t_{meas})$$

Furthermore the resolution σ_{res} is also a function of the measured time t_{meas} (see section 8).

The total sample likelihood L is obtained by summing over all event likelihoods, i.e.

$$L = \prod_{i}^{n} P(t_{meas}|r_{reco})_i$$

We used Minuit[24] (via the Root[15] TMinuit class) to minimise $-logL$ to obtain the best estimate of the RT-parameters and the parameters describing the resolution.

This RT-fit requires again an iterative and step-wise procedure, i.e. in order to reconstruct tracks we need an RT-relation and in order to determine the RT-relation we need reconstructed tracks. In the first step we use the integrated drift time spectrum as a source of an initial RT-relation. This is a valid approximation if a cell was uniformly irradiated (see [1]). With this initial RT-relation we can fit tracks and get the first set of measurements $(t_{meas}, r_{reco})_i$. These are used to perform the above likelihood fit resulting in a new set of parameters describing the RT-relation. We used a 3^{th} order spline with 6 parameters to describe the RT-relation. In figure 16 the RT-relations for several steps in the fit are shown.

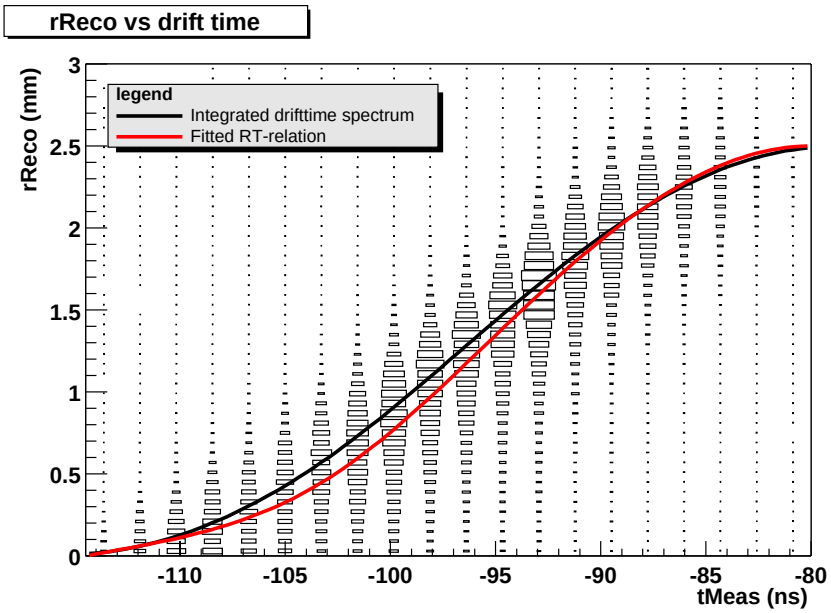

Figure 16: Initial and final RT-relation for 5 mm straw tubes of the standard run. The inititial RT relation is obtained from integrating the drift time spectrum. The final RT-relation is the relation obtained after the last step in the fitting procedure.

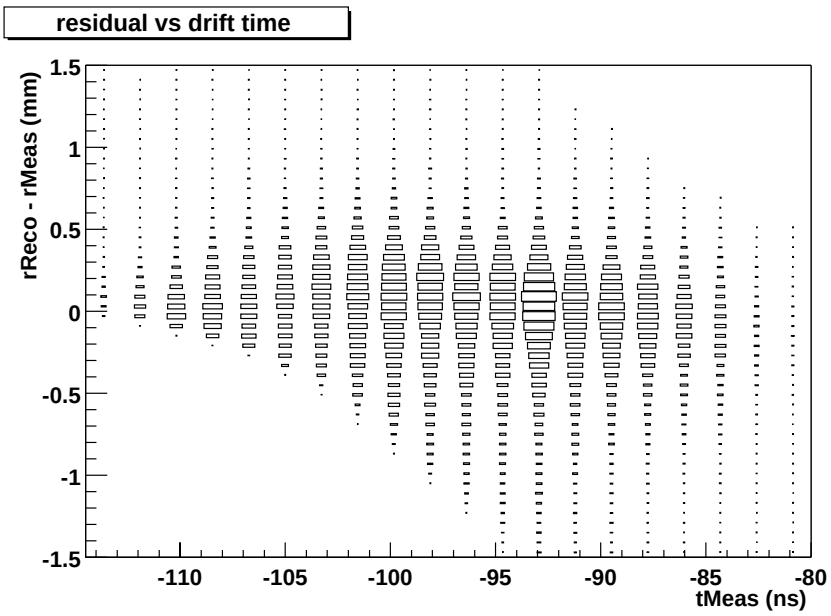

Figure 17: The residual of r_{reco} with the measured distance r_{meas} to the wire as a function of the measured drift time t_{meas} for a 5 mm straw tube in the standard run.

8 Resolution

In general words the resolution of a drift chamber is a measure of the average accuracy of the measurement. As noted in section 7 the quantity that one defines to be measured by a drift cell can be the drift time as well as the closest distance of the track to the wire, depending on the "application". In this note we use the track fit point of view. For a track fit a drift cell supplies a distance and an estimate of the error on this distance. The distance r_{meas} is obtained from the RT-relation as described in section 7. In the same manner we use a σ_{res}T-relation to get the best estimate of the error on the closest distance(σ_{res}) from the measured drift time t_{meas}.

In figure 17 the residual of the reconstructed closest distance of approach r_{reco} with the measured distance r_{meas} as a function of the measured drift time t_{meas} is shown. Note that, because a distance can never be negative and is also limited by the cell boundary of 2.5 mm, the scatter-plot contains two areas (bottom left and top right) that are excluded from data. Furthermore, as can be seen from the example residual distribution (in the time bin $t_{meas} \sim$ 93 ns) in figure 18, the resolution is none Gaussian and contains tails.

As mentioned, in the likelihood fit of section 7, we also fit a σ_{res}T-relation.

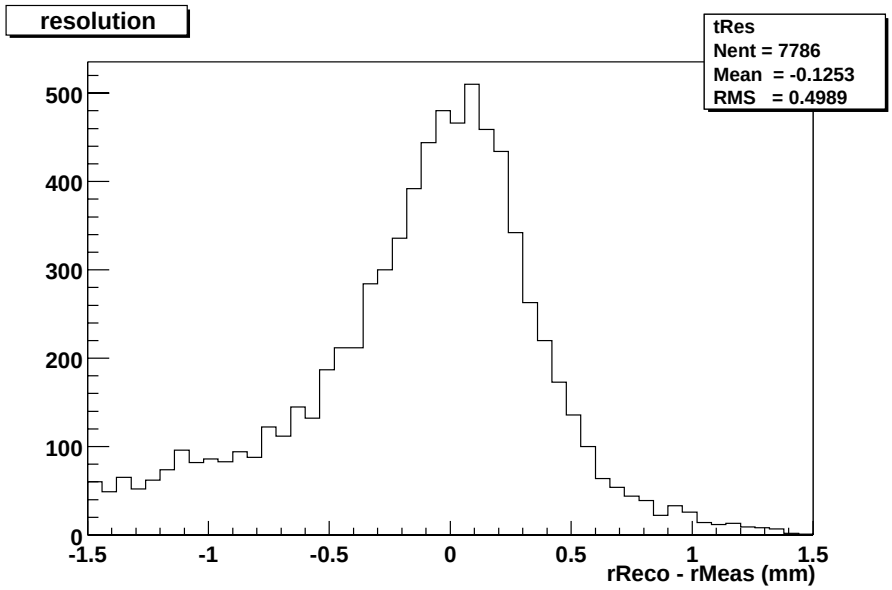

Figure 18: The residual of r_{reco} with the measured distance r_{meas} to the wire for $t_{meas} \sim 93$ ns in a 5 mm straw tube in the standard run.

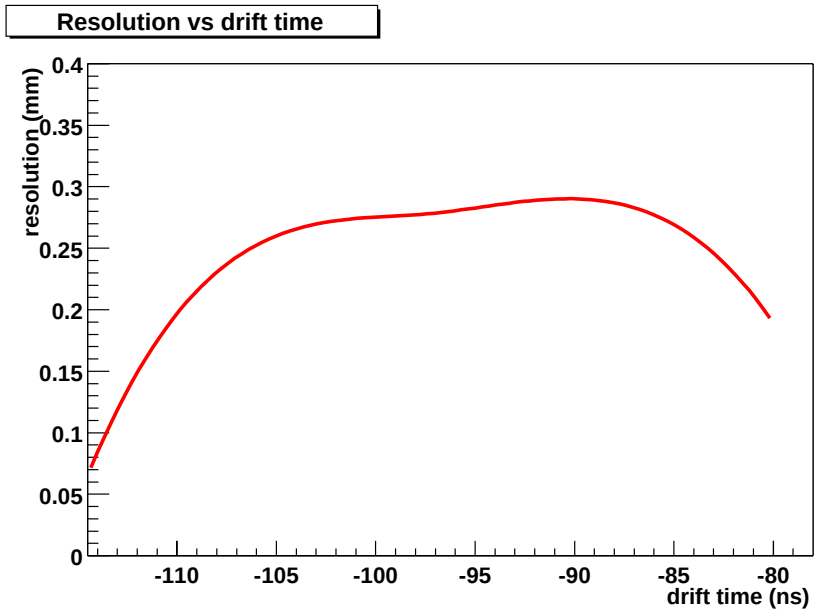

Figure 19: The fitted σ_{res}T-relation for the 5 mm straw tubes in the standard run.

To compensate for the none Gaussian and asymmetric behaviour we have added a flat background component to the probability term $P(t_{meas}|r_{real})$ in the fit. We used a 3^{th} order spline with 5 parameters to describe the relation. In figure 19 the final fitted σ_{res}T-relation is shown. For small drift times the error on the measured distance is small (75 μm) caused by the fact that the distance can not become negative. For the main part of the drift times the error on the measurement is above 260 μm. This is worse than the design resolution of 200 μm. A likely explanation for the bad resolution is a to high threshold in combination with a relatively low high voltage, as was the case due to the data acquisition problems mention in section 3.1. In that case the signal caused by the first primary cluster might be below threshold resulting in detection of later clusters. This hypothesis is confirmed by measurements in the May 2000 test beam[9].

[9]This data is reported in a separate note.

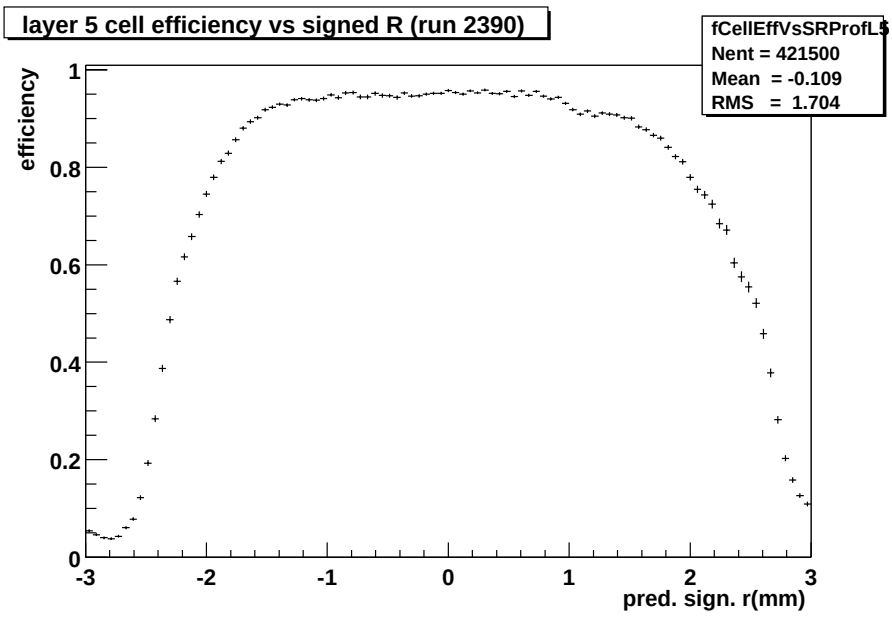

Figure 20: Efficiency as a function of predicted position in a cell for the standard run.

9 Efficiency

The exact efficiency of a detector can be defined in numerous ways. We follow [19] by defining the hit efficiency as the probability that a traversing ionising particle through a cell causes a signal in the data acquisition, i.e. a hit. In order to measure this quantity we have to determine if a particle went through a cell and if a hit was created. We again follow [19] and identify two types of hits, i.e. *measured hits* and *predicted hits* . Measured hits are hits present in the data acquisition (i.e. "on tape"). Predicted hits are hits predicted by the reconstructed tracks. Using these definitions we can estimate the efficiency as the fraction of predicted hits that is actually measured, i.e.

$$\text{Efficiency} = \frac{\text{measured hits}}{\text{predicted hits}}$$

In practice the efficiency is determined as follows. A track is reconstructed using all layers except the layer in which cell efficiencies are determined. This is needed to ensure that the efficiency is not biased by the information of the test layer. From the reconstructed track a prediction is made into the test layer, resulting in a distance to the predicted closest cell. If the closest cell is hit it is said to be 100% efficient for that distance, otherwise it is 0%

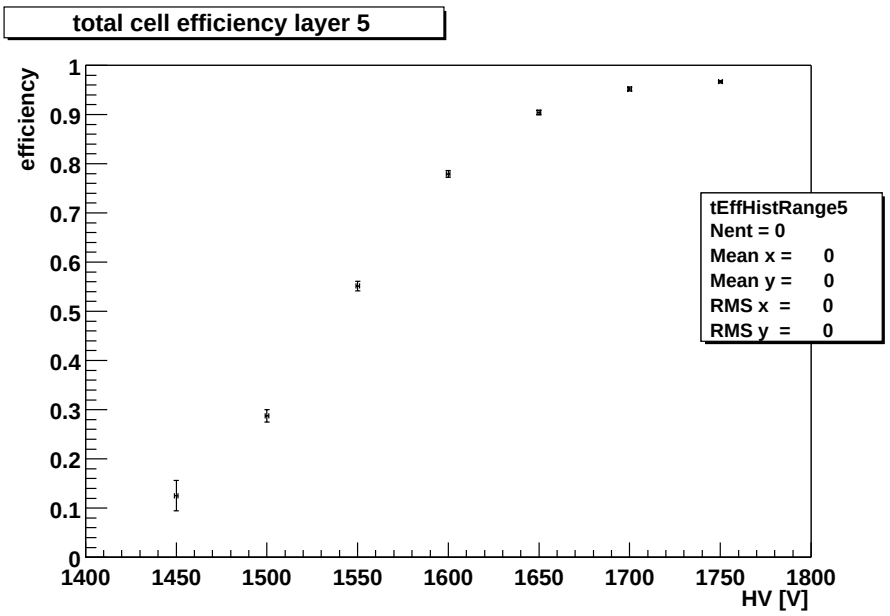

Figure 21: Average cell efficiency versus applied high voltage plateau for a 5 mm straw tube.

efficient for the event. By repeating this procedure for many events we get the efficiency as a function of the predicted position in a cell as shown in figure 20.

This figure shows several effects. First of all one sees that close to the cell edges (r=$\pm$2.5 mm) the efficiency is lower than in the main part of the cell. This can partly be explained by the fact that the track segment in the cell is short for particles traversing a cell close to its boundary (see e.g. [19]). Due to the limited precision in the track parameters of reconstructed tracks the position of the track through the cell is known with limited accuracy. This results in a smearing of the efficiency curve in figure 20, leading to an apparent efficiency outside of the cell boundary and an apparant extra decrease of efficiency close to the cell edges.

From an efficiency curve as shown in figure 20 we can calculate the average efficiency over the total cell range. In figure 21 the average efficiency as a function of the applied high voltage is presented. It becomes clear that the standard run at 1650 Volts (see section 3.2) was not operated at the fully achievable efficiency. The maximum efficiency is measured at 1750 Volts, i.e. $94.4 \pm 0.6\%$. To exclude boundary effects, in figure 22 the efficiency versus high voltage for the inner part of the cell is presented. A maximum efficiency of $98.6 \pm 0.4\%$ is achieved for 1700 V.

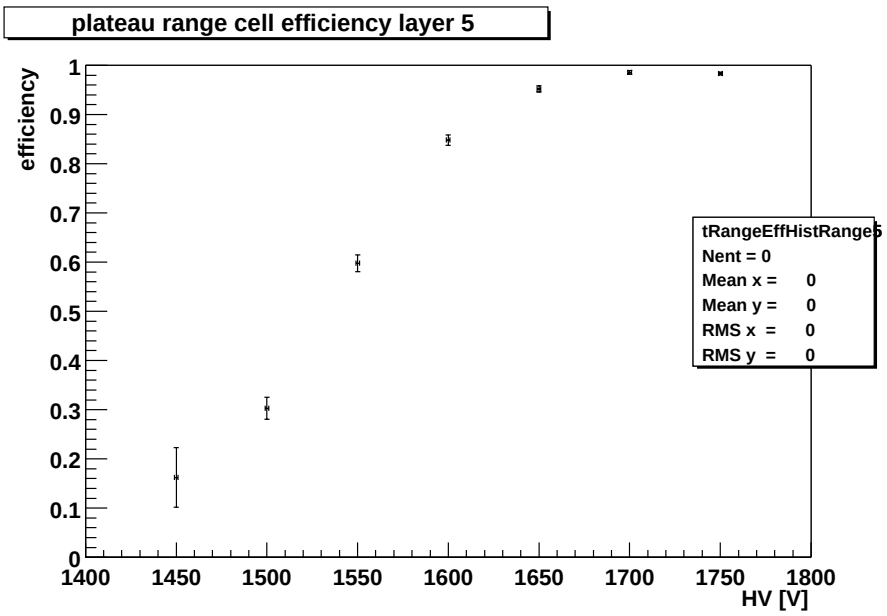

Figure 22: Cell efficiency as a function of the applied high voltage for a 5 mm straw tube ignoring edge effects.

In the procedure described above we can get a systematic error if we make a bias in the classification of hits. The presence of noise and cross talk makes that not all measured hits are true track signals. Noise hits could make the quoted efficiency too large. In section 10 noise and cross talk are dealt with in more detail. From the numbers presented there we expect this systematic error to be smaller than the statistical error. Opposed to this, not all predicted hits will be measured. As discussed in section 3.1 errors in the data acquisition caused a loss of hits without flagging the data for errors. Because this data acquisition inefficiency could not be fully reconstructed we can expect an underestimation of the cell efficiency.

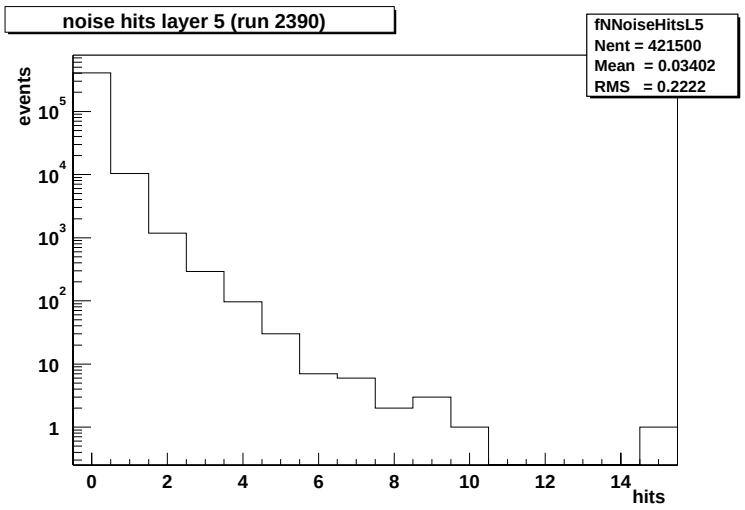

Figure 23: Distribution of the number of noise hits per event for a 5 mm straw layer (6032A) in the standard run.

10 Noise and cross-talk

There are numerous effects that can cause a hit to be registered although no particle crossed the detection cell. There are various sources of these *noise hits* e.g. pike-up, cross talk between channels and electronics oscillations. In order to quantify the amount of noise we define all hits that are *measured* but not *predicted*[10] to be noise hits. In practise a measured hit is considered not predicted if the residual of predicted distance and measured distance to the wire is larger than 3.0 mm. In order to avoid unnecessary complications we also only select events with one reconstructed track.

Figure 23 shows the distribution of the number of noise hits in a specific single layer. For this layer the average number of noise hits per event is 0.034 for the whole layer, which corresponds to a probability of 0.22% to have a noise hit in a single cell. It turned out that the number of noise hits strongly depends on the layer tested. In order to understand the sources of the noise hits we investigated the time structure w.r.t. other hits. In particular we plot the time difference between a hit assigned to a track and a noise hit in the same layer.

Figure 24 shows the drift time difference of noise hits w.r.t. the signal hit for 5 mm straw tubes in the standard run. We see a distribution of ∼40 ns width around zero, a peak at + ∼20 ns and a flat tail to larger times. We

[10]See section 9 for the used definition for *measured* and *predicted* hits.

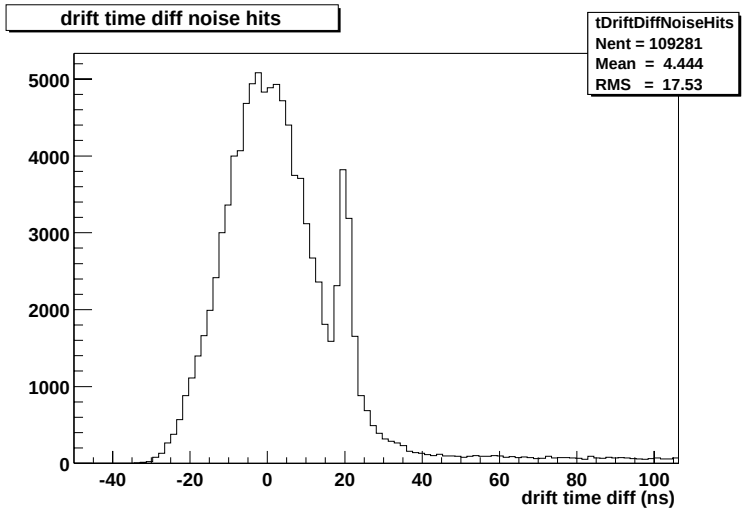

Figure 24: Drift time difference of noise hits w.r.t. signal hits in 5 mm straw tubes of the standard run.

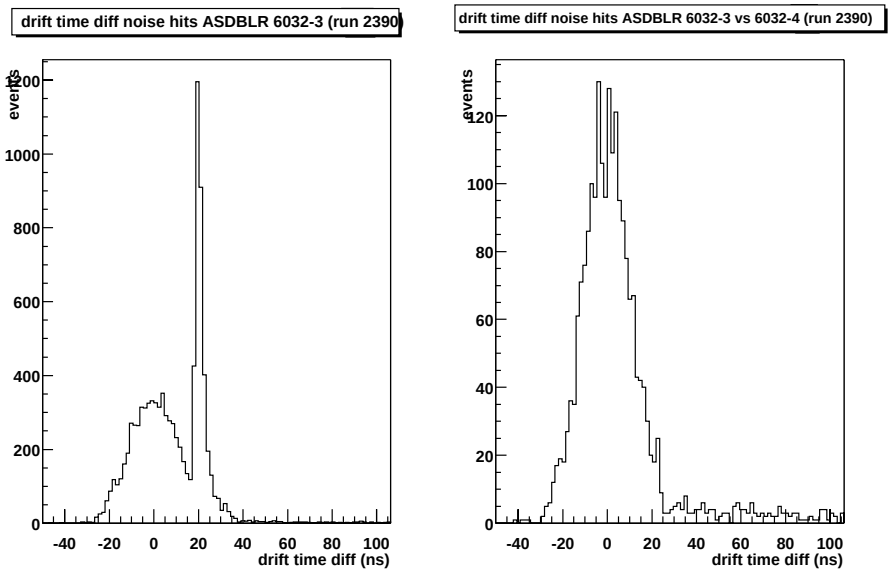

Figure 25: Drift time difference of noise hits w.r.t. signal hits in 5mm straw tubes of mono layer 6032B in the standard run. A) Shows the difference in drift time for noise hits in the same ASDBLR chip as the signal hit. B) Shows the difference in drift time for noise hits in the ASDBLR chip adjacent to the ASDBLR chip of the signal hit in the same layer.

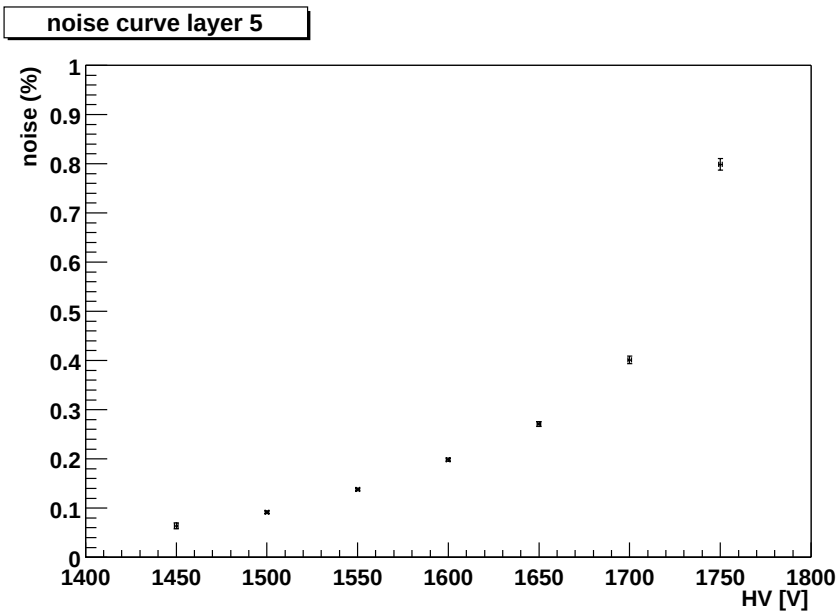

Figure 26: The average probability for a single cell to contain a noise hit as a function of the applied high voltage for 5 mm straw tube drift cells with gas mixture Ar:CF_4:CO_2(68:27:05), no magnetic field and a treshold of 6 fC in the 1999 testbeam.

do not see a sharp peak at 0ns which we would expect from 'normal' cross talk. The peak at 20 ns is surprising. It indicates some sort of oscillations or delayed cross talk. Further study shows that this correlation only occurs between channels on the same ASDBLR chip as can be seen in figure 25. Figure 25-A shows the difference in drift time within one ASDBLR chip, figure 25-B the difference in drift time between two different, but neighbouring, ASDBLR chips. A dedicated electronics study[8] confirms that for a number of ASDBLR chips extra signals can be created on all other 7 channels if the pulse height on one of the inputs is high (larger than $\sim$50 fC for a 2 fC threshold). The percentage of noise hits per ASDBLR chip has been shown to vary between 1.3% and 4.5% in the standard run.

Figure 26 shows the average number of noise hits per cell as a function of the applied high voltage for the 5 mm straw tubes in the 1999 testbeam. At 1750V this number is close to 1%. As mentioned the *after pulsing* caused by the ASDBLR depends largely on the chips chosen. Selecting goods chips should significantly reduce this number.

11 Conclusions

The data of the 1998 and 1998 test beam periods has been analysed. The electronics was newly developed and in fact still undergoing field testing. Problems with the electronics severely restricted the data quality. Data of better quality is obtained in 2000 and will be described in a seperate note. The description of analysis methods given in this note also applies to the 2000 data. In spite of the limitations, the 1998 and 1999 data have led to important conclusions:

- No 8 mm cells can be used in LHCb because the maximum drift time becomes to large to stay within two bunchcrossings.
- Straw tube drift cells with a 5 mm diameter, with gas mixture Ar:CF_4:CO_2 (68:27:05) are fast enough upto a magnetic field of 1.6 Tesla. This is sufficient for all chamber positions within LHCb.
- The efficiency of 5 mm straw tubes prototypes is $> 98\%$ at a high voltage of 1700 Volt in the gas mixture Ar:CF_4:CO_2 (68:27:05).

References

[1] H. Tolsma, "The Honeycomb Strip Chamber", PhD thesis, Universiteit Twente, 1996.

[2] F.Sauli, "Principles of operation of multiwire proportional and drift chambers", CERN 77-09, 1977.

[3] G.W. van Apeldoorn, "Test beam guide", internal LHCb Outer Tracker note, 1998.

[4] F. Blekman, "Carbon-coated drift chambers: An ageing experiment", University of Amsterdam graduation thesis, 2000.

[5] G.W. van Apeldoorn, "Test beam guide", internal LHCb Outer Tracker note, 1999.

[6] T.Sluijk et al., "The Beam Test Electronics for the LHCb Outer Tracker", NIKHEF ETR 00-02-15, 2000.

[7] B. Bevensee et al., "A Amplifier Shaper Discriminator with Baseline Restoration for the Atlas Transition Radiation Tracker", IEEE Transactions on Nuclear Science, vol 43, 1996.

[8] V. Gromov, "Study of operational properties of the ASDBLR chip for the LHCb Outer Tracker.", LHCb 2000-054, 2000.

[9] J.D.Schipper, P Rewiersma, "Datimizer", http://www.nikhef.nl/user-/jds/datcha/Datimizer.pdf

[10] J. Christiansen, "32 Channel TDC with on chip buffering and trigger matching", CERN-LHCC-97-60, 1997.

[11] JTAG Technologies B.V, http://www.jtag.com/, 2000.

[12] H. Groenstege et al., "16 Channel read out driver for the Drift Chambers used in L3+Cosmics project", http://www.nikhef.nl/pub/departments-/et/L3/cosmics/nimrod/nimrod.pdf, 1999.

[13] J.D. Schipper, P. Rewiersma, "DDAQT version DATIMIZER 980706", http://www.nikhef.nl/user/jds/datcha/ddaqtv2.pdf, 1998.

[14] R. van Wijk, "DAQFIT a scalable DAQ system", http://www.nikhef.nl-/user/ruud/HTML/daqfit.html, 2000.

[15] R. Brun and F. Rademakers, "ROOT - An Object Oriented Data Analysis Framework", Proceedings AIHENP'96 Workshop, Lausanne, Sep. 1996, Nucl. Inst. & Meth. in Phys. Res. A 389 (1997) 81-86. See also http://root.cern.ch/.

[16] LHCb Software Architecture group, Editor: P. Mato, "GAUDI, LHCb data processing applications framework - Architecture design document", LHCb 98-064, 1998.

[17] R. van der Eijk, "LHCb Outer Tracker Testbeam Software (Online) Monitoring, Control and Analyses software", http://home.cern.ch-/lhcbott/software/Index.html, 1999.

[18] R. Veenhof, "Garfield, simulation of gaseous detectors", CERN writeup W5050 (User Guide V6.31), 1999.

[19] W. Hulsbergen et al., "Calibration of Hera-B Outer Tracker Chambers in a Cosmic Ray Setup at NIKHEF", HERA-B 00-014, 2000.

[20] R.E.Kalman, Trans. ASME, J. Basic Engineering, 1960.

[21] R.K. Bock et al., "Data analysis techniques for high-energy physics experiments", Cambridge Univ. Press, 1990.

[22] R. Mankel, "Application of the Kalman Filter Technique in the HERA-B Track Reconstruction", HERA-B 95-239, 1995.

[23] R. Mankel, "ranger - a Pattern Recognition Algorithm for the HERA-B Main Tracking System", HERA-B 97-82, 1997.

[24] F. James, "Minuit, Function Minimization and error analysis", CERN writeup D506 (Reference Manual V94.1), 1994.